

# Magnetocrystalline anisotropy in $\text{RAu}_2\text{Ge}_2$ ( $\text{R} = \text{La}, \text{Ce}$ and $\text{Pr}$ ) single crystals

Devang A. Joshi and A. K. Nigam, S. K. Dhar and A. Thamizhavel  
*Department of Condensed Matter Physics and Materials Science,  
 Tata Institute of Fundamental Research, Colaba, Mumbai 400 005, India.*

Anisotropic magnetic properties of single crystalline  $\text{RAu}_2\text{Ge}_2$  ( $\text{R} = \text{La}, \text{Ce}$  and  $\text{Pr}$ ) compounds are reported.  $\text{LaAu}_2\text{Ge}_2$  exhibit a Pauli-paramagnetic behavior whereas  $\text{CeAu}_2\text{Ge}_2$  and  $\text{PrAu}_2\text{Ge}_2$  show an antiferromagnetic ordering with Neel temperatures  $T_N = 13.5$  and  $9$  K, respectively. The anisotropic magnetic response of Ce and Pr compounds establishes  $[001]$  as the easy axis of magnetization and a sharp spin-flip type metamagnetic transition is observed in the magnetic isotherms. The resistance and magnetoresistance behavior of these compounds, in particular  $\text{LaAu}_2\text{Ge}_2$ , indicate an anisotropic Fermi surface. The magnetoresistivity of  $\text{CeAu}_2\text{Ge}_2$  apparently reveals the presence of a residual Kondo interaction. A crystal electric field analysis of the anisotropic susceptibility in conjunction with the experimentally inferred Schottky heat capacity enables us to propose a crystal electric field level scheme for Ce and Pr compounds. For  $\text{CeAu}_2\text{Ge}_2$  our values are in excellent agreement with the previous reports on neutron diffraction. The heat capacity data in  $\text{LaAu}_2\text{Ge}_2$  show clearly the existence of Einstein contribution to the heat capacity.

PACS numbers: 71.70.Ch, 72.15.Eb, 73.43.Qt, 75.50.Ee

Keywords: Single Crystal, Crystal Electric Field,  $\text{RAu}_2\text{Ge}_2$ , Antiferromagnets

## I. INTRODUCTION

The family of rare earth intermetallic compounds  $\text{RT}_2\text{X}_2$  ( $\text{R}$ : rare earths,  $\text{T}$ : Transition metal and  $\text{X}$ : p-block element (Si or Ge)) crystallizing in the  $\text{ThCr}_2\text{Si}_2$ -type tetragonal structure constitute a reservoir of compounds showing a wide variety of interesting magnetic and superconducting properties. Some of the Ce and Yb based compounds within this family are well-known for their heavy fermion, valence fluctuation, quantum criticality, superconductivity and Kondo behavior arising from the hybridization between the  $4f$  and the conduction electrons. For example  $\text{CeCu}_2\text{Si}_2$  [1] is a well known first heavy fermion superconductor,  $\text{CeCu}_2\text{Ge}_2$  shows Kondo behavior [2],  $\text{CeRu}_2\text{Si}_2$  [3],  $\text{CePd}_2\text{Si}_2$  [4],  $\text{CeCu}_2\text{Ge}_2$  [5] and  $\text{CeRh}_2\text{Si}_2$  [6] show a quantum critical behavior.  $\text{YbRh}_2\text{Si}_2$  possessing a low lying antiferromagnetic ground state has been intensively studied in recent years for its quantum critical behavior induced both by external magnetic field and pressure. Different types of magnetic ordering are observed in the Pr compounds.  $\text{PrRu}_2\text{Si}_2$  [8],  $\text{PrRu}_2\text{Ge}_2$  [9] and  $\text{PrOs}_2\text{Si}_2$  [14] are ferromagnetic while antiferromagnetic or complicated magnetic ordering is observed in case of  $\text{PrCo}_2\text{Ge}_2$  [10],  $\text{PrCo}_2\text{Si}_2$  [11],  $\text{PrNi}_2\text{Si}_2$  [12] and  $\text{PrCu}_2\text{Ge}_2$  [13]. While initial reports are typically based on polycrystalline materials, data obtained on single crystals provide a more comprehensive picture of the physical properties including their anisotropy, inevitable in tetragonal symmetry. For example, our recent work on a single crystal of  $\text{CeAg}_2\text{Ge}_2$  [7] removed the ambiguity about the magnetic transition temperature of this compound which existed due to the conflicting reports

in the literature based on polycrystalline samples. A quasi-quartet ground state arising due to two low lying crystal electric field split states was also established from the analysis of the magnetization data which show a large anisotropy along the two principle crystallographic directions. The successful growth of single crystals of  $\text{CeAg}_2\text{Ge}_2$  [7] achieved for the first time motivated us to investigate the single crystalline behavior of  $\text{RAu}_2\text{Ge}_2$  ( $\text{R} = \text{La}, \text{Ce}$  and  $\text{Pr}$ ) compounds using magnetic, thermal and transport measurements down to  $1.8$  K.

In this paper, findings of the detailed study of the physical properties of single crystalline  $\text{RAu}_2\text{Ge}_2$  ( $\text{R} = \text{La}, \text{Ce}$  and  $\text{Pr}$ ) compounds is reported. Polycrystalline  $\text{CeAu}_2\text{Ge}_2$  and  $\text{PrAu}_2\text{Ge}_2$  have previously been reported to order antiferromagnetically at  $T_N = 16$  K [15] and  $12$  K [16] respectively. The neutron diffraction results on  $\text{CeAu}_2\text{Ge}_2$  clarifies the pure antiferromagnetic ordering of the Ce moment lying along the  $c$  axis of the tetragonal unit cell with an ordered moment of  $1.88 \mu_B/\text{Ce}$  at  $1.5$  K.  $\text{PrAu}_2\text{Ge}_2$  undergoes a metamagnetic transition at  $32$  KOe [16]. There are no reports on  $\text{LaAu}_2\text{Ge}_2$ . Our study on single crystalline samples infers the ordering temperatures of the compounds to be  $13.5$  and  $9$  K for  $\text{CeAu}_2\text{Ge}_2$  and  $\text{PrAu}_2\text{Ge}_2$  respectively in contrast to the polycrystalline report. Other results on  $\text{CeAu}_2\text{Ge}_2$  are in agreement with the reported ones. In case of  $\text{PrAu}_2\text{Ge}_2$  spin flip type metamagnetic transition occurs at  $22$  KOe in contrast to the polycrystalline report.

## II. EXPERIMENTAL

Single crystals of  $\text{RAu}_2\text{Ge}_2$  compounds were grown by high temperature solution growth method. Since all the constituents of  $\text{RAu}_2\text{Ge}_2$  have high melting points, none of them could be used as a flux. Looking into the binary phase diagram of the Au:Ge system, it was observed

---

Electronic address: devang@tifr.res.in

that for a particular composition of Au:Ge = 72:28, an eutectic forms with a melting point of 361 °C. Since we had previously succeeded in growing the single crystals of CeAg<sub>2</sub>Ge<sub>2</sub> by using a binary Ag-Ge eutectic as a self flux, initially we attempted Au-Ge eutectic for the growth of RAu<sub>2</sub>Ge<sub>2</sub> compounds. But the single crystals thus obtained were small in size. We also attempted to grow the single crystals of RAu<sub>2</sub>Ge<sub>2</sub> compounds using Bi as flux. To avoid the reaction of flux with the constituents of compounds, an ingot of RAu<sub>2</sub>Ge<sub>2</sub> was prepared by melting in an arc furnace with the constituents taken in proper stoichiometric ratio. The as-cast ingot of RAu<sub>2</sub>Ge<sub>2</sub> and the Bi flux in the ratio of 1:19 were placed in an alumina crucible and subsequently sealed in an evacuated quartz tube. The mixture was heated up to 1100°C and maintained at that temperature for 30 hrs, followed by slow cooling (1°C / h) to 550°C and then rapidly cooled down to room temperature. The crystals were separated from the flux by means of centrifuging. The typical size of the obtained crystals was 7 × 4 × 1 mm<sup>3</sup>. The crystals nucleated on the walls of crucible and formed as thin platelets sticking together to form a big single crystal. An energy dispersive x-ray analysis EDAX was performed on all of the obtained single crystals to identify their phase. The EDAX results confirmed the crystals to be of the composition 1:2:2. In our present study we have used the single crystals grown from the Bi flux. To check for the phase purity, powder x-ray diffraction pattern of these compounds were recorded by powdering a few small pieces of single crystals. The grown crystals were then oriented along the principal crystallographic directions by means of Laue diffraction. Well defined Laue diffraction spots, together with the tetragonal symmetry pattern, indicated the good quality of single crystals. The crystals were then cut along the crystallographic directions using a spark erosion cutting machine to study their anisotropic properties. The DC magnetic measurements were performed in the temperature range 1.8 - 300 K and in the magnetic fields up to 120 KOe along the two principal directions using a SQUID magnetometer (Quantum Design) and a vibrating sample magnetometer (VSM, Oxford Instruments). The resistivity and heat capacity were measured using a physical property measurement system (PPMS, Quantum Design).

### III. RESULTS AND DISCUSSION

The RAu<sub>2</sub>Ge<sub>2</sub> (R = La, Ce and Pr) compounds form in a tetragonal structure with a space group *I*4/*mmm*. To confirm the phase homogeneity of the compounds with proper lattice and crystallographic parameters, a Rietveld analysis of the observed x-ray pattern of the three compounds was carried out using the FULLPROF program [17]. The lattice parameters and the unit cell volume thus obtained are listed in Table I and a representative Rietveld refined plot of CeAu<sub>2</sub>Ge<sub>2</sub> is shown in Fig. 1. We obtained a  $\chi^2$  value of 2.6, goodness of fit of

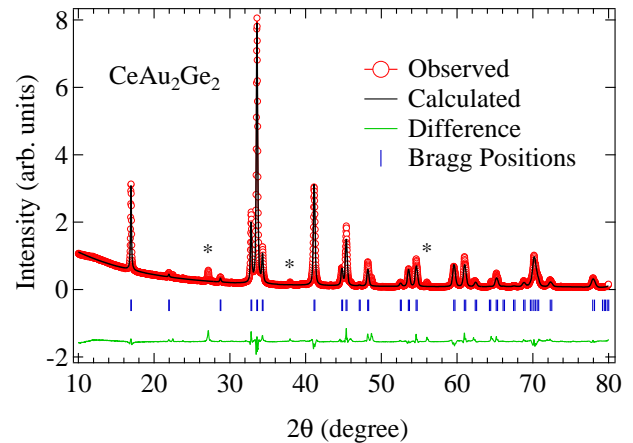


Figure 1: (Color online) Powder x-ray diffraction pattern recorded for crushed single crystals of CeAu<sub>2</sub>Ge<sub>2</sub> at room temperature. The solid line through the experimental data points is the Rietveld refinement profile calculated for the tetragonal CeAu<sub>2</sub>Ge<sub>2</sub>. The stars represent the x-ray peaks corresponding to Bi.

Compound	<i>a</i> (Å)	<i>c</i> (Å)	<i>V</i> (Å <sup>3</sup> )	<i>T<sub>N</sub></i> (K)
LaAu <sub>2</sub> Ge <sub>2</sub>	4.422	10.45	204.3	P-P
CeAu <sub>2</sub> Ge <sub>2</sub>	4.385	10.444	200.8	13.5
PrAu <sub>2</sub> Ge <sub>2</sub>	4.366	10.443	199	9.0

Table I: Lattice parameters of RAu<sub>2</sub>Ge<sub>2</sub> compounds with unit cell volume and Neel temperature. P-P: Pauli paramagnetic.

1.7, and Bragg R factor of 0.081. The lattice parameters are comparable to those reported earlier for the polycrystalline samples [15, 16]. The lattice parameters decrease as we move from La to Pr, attributed to well known lanthanide contraction. The unit cell volume of RAu<sub>2</sub>Ge<sub>2</sub> compounds is higher compared to that of RCu<sub>2</sub>Ge<sub>2</sub> compounds and less than that of RAg<sub>2</sub>Ge<sub>2</sub> compounds. This may be due to the intermediate size of the Au atom compared to Cu and Ag.

#### A. LaAu<sub>2</sub>Ge<sub>2</sub>

We first describe the physical properties of LaAu<sub>2</sub>Ge<sub>2</sub> which can be considered as the reference, non-magnetic analog for the magnetic RAu<sub>2</sub>Ge<sub>2</sub> compounds. The susceptibility of LaAu<sub>2</sub>Ge<sub>2</sub> (Fig. 2a) shows a Pauli-paramagnetic behavior at room temperature, with an absolute value of nearly  $2.3 \times 10^{-4}$  emu/mol. It remains nearly temperature independent down to 50 K and shows an upturn at lower temperatures (Fig. 2a). The low temperature upturn is most likely due to the presence of paramagnetic ions in the constituents used to prepare the alloys. A fit (shown by the solid line in Fig. 2a) of

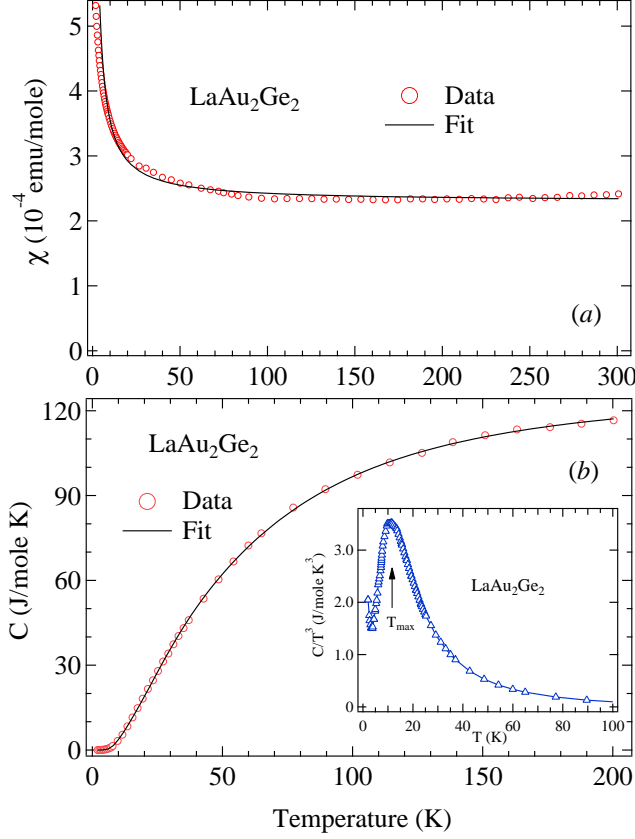


Figure 2: (Color online) a) Magnetic susceptibility of  $\text{LaAu}_2\text{Ge}_2$  with a fit described in text. The inset shows the  $C/T$  vs  $T^2$  plot with a linear fit. b) Heat capacity curve of  $\text{LaAu}_2\text{Ge}_2$  with a fit described in the text. The inset shows the  $C/T^3$  vs  $T$  plot.

the modified Curie-Weiss law

$$\chi = \chi_0 + \frac{N \mu_{\text{eff}}^2}{3k_B (T - T_p)} \quad (1)$$

to the data, where the parameters have their usual meaning, yields  $\chi_0 = 2.312 \times 10^{-4}$  emu/mol and  $\mu_{\text{eff}} = 0.1 \mu_B$ . The magnitude of  $\chi_0$  is typical for the La compounds and a low value of the effective moment indicates that the upturn at low temperatures is due to the presence of some ( $< 1\%$ ) magnetic impurity ions in the constituents. The heat capacity of the compound (Fig. 2b) increases monotonically with temperature. The magnitude of the electronic contribution  $\gamma$ , obtained from the low temperature heat capacity data is  $7 \text{ mJ/mol K}^2$ . Inset of Fig. 2b shows a plot of  $C/T^3$  vs  $T$ , a representation that is often used to assess the possible presence of low-frequency Einstein modes in the specific heat [19]. The maximum, in this case at  $T_{\text{max}} = 13 \text{ K}$ , could be interpreted as the temperature below which the Einstein modes are frozen out. This is also the temperature where the deviation from a pure Debye description of the specific heat becomes conspicuous. Considering this, the

thermal variation of the heat capacity of the compound was fitted to the combined Einstein and Debye contributions as shown by the solid line in Fig. 2b. The total heat capacity in such a case is given by

$$C_{\text{Tot}} = \gamma T + (C_E + C_D) \quad (2)$$

where the first term represents the electronic contribution, the second term includes Einstein contribution  $C_E$  and Debye contribution  $C_D$ . The Einstein contribution is given by

$$C_E = \sum_{n^0}^X 3n_E n^0 R \frac{y^2 e^y}{(e^y - 1)^2} \quad (3)$$

where  $y = \theta_E/n^0 = T/\theta_E$ ,  $\theta_E$  is the Einstein temperature,  $n^0$  is the summation over the different Einstein temperatures,  $R$  is the gas constant and  $n_E$  is the number of Einstein oscillators. The Debye contribution is given by

$$C_D = 9n_D R \left( \frac{T}{\theta_D} \right)^3 \int_0^{\theta_D/T} \frac{x^4 e^x dx}{(e^x - 1)^2} \quad (4)$$

where  $x = \theta_D/T$ ,  $\theta_D$  is the Debye temperature and  $n_D$  is the number of Debye oscillators. Iterative fit to the Eq. 2 was performed by using the values of electronic contribution  $\gamma$  as estimated above and fixing the number of atoms  $n_D$  and  $n_E$  for a particular fit, allowing both  $\theta_E/n^0$  and  $\theta_D$  to vary as fitting parameters. A good fit to the heat capacity of  $\text{LaAu}_2\text{Ge}_2$  over the entire range of temperature was obtained by assigning three Debye characteristic atoms ( $n_D = 3$ ) with  $\theta_D = 305 \text{ K}$  plus two Einstein characteristic atoms ( $n_{E1} = n_{E2} = 1$ ) with  $\theta_{E1} = 74 \text{ K}$ . The description of heat capacity in terms of a combination of acoustic and optical modes can be readily understood by assigning the La and Ge atoms in the unit cell to three Debye characteristic modes and Au to the remaining Einstein modes. Since Au is much larger in size compared to other atoms, it can be expected to vibrate with a lower natural frequency. It can be shown that the Einstein temperature  $\theta_E$  is related to the peak in  $C/T^3$  against  $T$  plot ( $T_{\text{max}}$ ) by the relation  $T_{\text{max}} = \theta_E/5$  [20], which is in fair agreement with the observed value of  $T_{\text{max}} = 13 \text{ K}$ .

The resistivity of  $\text{LaAu}_2\text{Ge}_2$  with current parallel to [100] and [001] directions is shown in Fig. 3. The resistivity along both the crystallographic directions exhibit a metallic behavior down to 15 K and levels off at low temperatures with a residual resistivity of  $18 \mu\Omega$  and  $1.4 \mu\Omega$  respectively for [100] and [001] directions. The observed behavior is in tune with the phonon induced scattering of the charge carriers as expected for a non magnetic compound. The resistivity along [001] direction is found to be lower compared to the in-plane [100] resistivity by a factor of nearly 20 at 300 K points out significant anisotropy. The similar anisotropic behavior in the resistivity was also found for Ce and Pr compounds

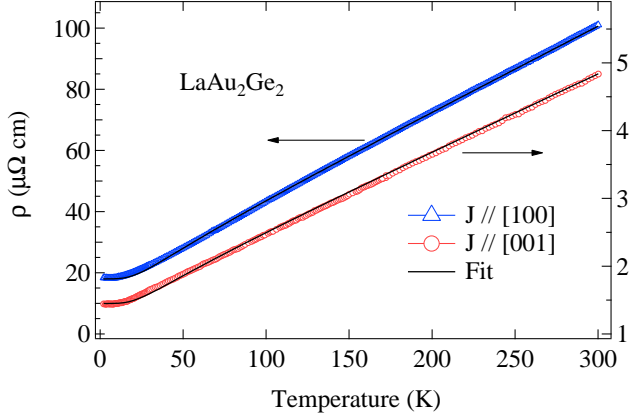


Figure 3: (Color online) Resistivity of  $\text{LaAu}_2\text{Ge}_2$  with current parallel to [100] and [001] directions. The resistivity along the two directions is fitted to Bloch-Grüneisen relation.

described below and may arise due to the inherent structural anisotropy of the compound. The resistivity with current parallel to the two crystallographic directions was fitted to the modified Bloch-Grüneisen relation given by

$$\rho(T) = \rho_0 + 4 \frac{D}{D} R \frac{T}{D} \int_0^{\frac{D}{T}} \frac{x^5 dx}{(e^x - 1)(1 + e^{-x})} \quad \text{K T}^3 \quad (5)$$

where  $x = \frac{D}{T}$ ,  $D$  is the Debye temperature,  $\rho_0$  is the temperature independent residual resistivity and  $R$  and  $K$  are the coefficients of the phonon contribution to the resistivity (second term) and the Mott  $s$ - $d$  inter band scattering (third term) respectively. The fit to the resistivity curves yields  $D = 126$  K,  $\rho_0 = 18 \text{ } \mu\Omega\text{cm}$ , and  $R = 0.273 \text{ } \mu\Omega\text{cm}$  for  $J // [100]$  and  $D = 125$  K,  $\rho_0 = 1.4 \text{ } \mu\Omega\text{cm}$  and  $R = 0.011 \text{ } \mu\Omega\text{cm}$  for  $J // [001]$ , the value of  $K$  was found to be zero for both the directions. The Debye temperature remains nearly same but there is an order of decrease in the magnitude of phonon contribution to the resistivity for  $J // [001]$  inferred from the values of  $R$ . The Debye temperature in the Bloch-Grüneisen relation often differs from the value of  $D$  obtained from heat capacity data. In principle, the value of  $D$  obtained from Bloch-Grüneisen relation should considerably differ from that obtained from heat capacity because the former takes into account only the longitudinal phonons [21].

### B. $\text{CeAu}_2\text{Ge}_2$

Figure 4a shows the magnetic susceptibility of  $\text{CeAu}_2\text{Ge}_2$  from 1.8 K to 300 K in a magnetic field of 3 kOe along the two crystallographic directions ([100] and [001]). The susceptibility with field parallel to [001] direction shows an antiferromagnetic transition at  $T_N = 13.5$  K, less than that observed from neutron

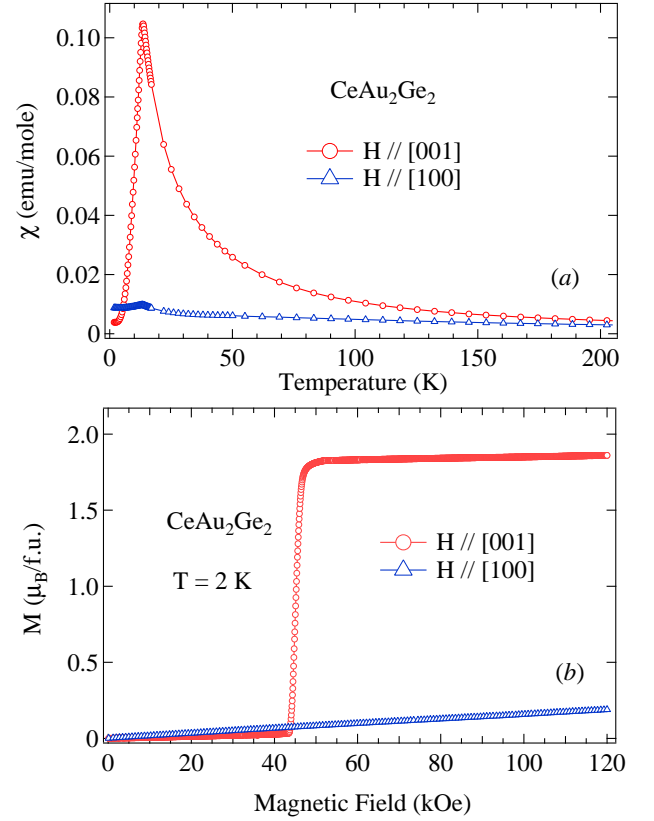


Figure 4: (Color online) a) Magnetic susceptibility of  $\text{CeAu}_2\text{Ge}_2$  with magnetic field (3kOe) applied along the two crystallographic directions. b) Magnetic isotherm at 2 K for the same with field along both the crystallographic directions.

diffraction on a polycrystalline sample (16 K) [15]. The sharp drop of susceptibility below the Neel temperature indicates that the moments are aligned antiferromagnetically along the [001] direction in possibly a collinear arrangement. The behavior indicates that the [001] axis is the easy axis of magnetization for  $\text{CeAu}_2\text{Ge}_2$  as reported by Loidl *et al* [15]. With field along [100] direction, the susceptibility remains below that of [001] direction in the entire temperature range followed by a Kink at the ordering temperature, indicating the hard axis of magnetization. Curie-Weiss fits of the inverse susceptibility in the paramagnetic state gives effective moment ( $\mu_B$ ) and paramagnetic Curie temperature ( $T_p$ ) as  $2.54 \text{ } \mu_B/\text{Ce}$  and  $2.54 \text{ } \mu_B/\text{Ce}$  and -63 K and 27 K for field parallel to [100] and [001] directions, respectively. The obtained effective moment for both the axes is equal to the expected theoretical value ( $2.54 \text{ } \mu_B/\text{Ce}$ ). The polycrystalline average of  $T_p$  is -34 K, which is in tune with the antiferromagnetic nature of this compound. The large negative value also indicates the presence of possible Kondo interaction. The magnetic isotherms of the compound with field along both the crystallographic directions ([100] and [001]) are shown in Fig. 4b. The linear behavior of the magnetization at

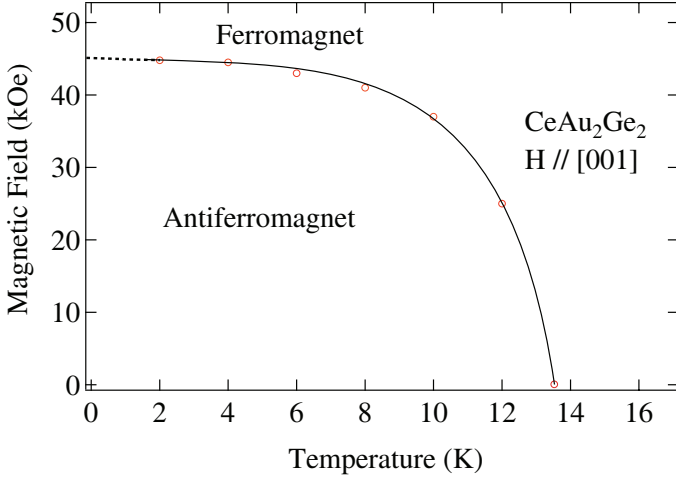


Figure 5: (Color online) Magnetic Phase Diagram of  $\text{CeAu}_2\text{Ge}_2$ .

2 K and up to 43 kOe with the field along [001] axis confirms the antiferromagnetic nature of the compound in the magnetically ordered state. The magnetization undergoes a spin flip type metamagnetic transition at the critical field  $H_c$  43 kOe followed by near saturation at high fields. The saturation moment obtained at 2 K and 120 KOe is  $1.86 \mu_B$ , less than the theoretical saturation moment of  $2.14 \mu_B$  and is in agreement with the neutron diffraction results [15]. From the differential plots of the isothermal magnetization curves (not shown here), we have constructed the magnetic phase diagram as depicted in Fig. 5. The critical field  $H_c$  decreases with increase in temperature and finally vanishes at  $T_N$ . At low temperatures and for fields less than 45 KOe, the system is in a purely antiferromagnetic state as indicated and enters into the field induced ferromagnetic state at higher fields.

The heat capacity behavior of the compound in zero and applied fields is shown in Fig. 6. An anomaly in the heat capacity at 13.5 K with a peak height of 11 J/mol K confirms the bulk magnetic ordering of  $\text{Ce}^{3+}$  ions. The peak height is close to the mean field value of 12.5 J/mol K for spin  $S = 1/2$ . The magnitude of the Sommerfeld coefficient was estimated to be 15 mJ/mol  $\text{K}^2$  from the  $y$  intercept of the  $C/T$  vs  $T^2$  curve (not shown). Application of the magnetic field of 20 KOe shifts the heat capacity peak towards low temperature and reduces its height. At higher fields (60 and 80 KOe) the peak vanishes altogether consistent with the presence of metamagnetic transition (43 KOe). The  $4f$  contribution to the heat capacity of  $\text{CeAu}_2\text{Ge}_2$   $C_{4f}$ , Fig. 6b was extracted by subtracting the heat capacity of  $\text{LaAu}_2\text{Ge}_2$ . Besides the peak at  $T_N$ ,  $C_{4f}$  exhibits a broad peak centered around 60 K arising due to the Schottky contribution from the thermal variation of the population of excited CEF levels. The entropy calculated using the expression  $S_{4f} = \int_0^T \frac{C_{4f}}{T} dT$ , plotted as a function of

temperature is shown in the inset of Fig. 6a. The entropy

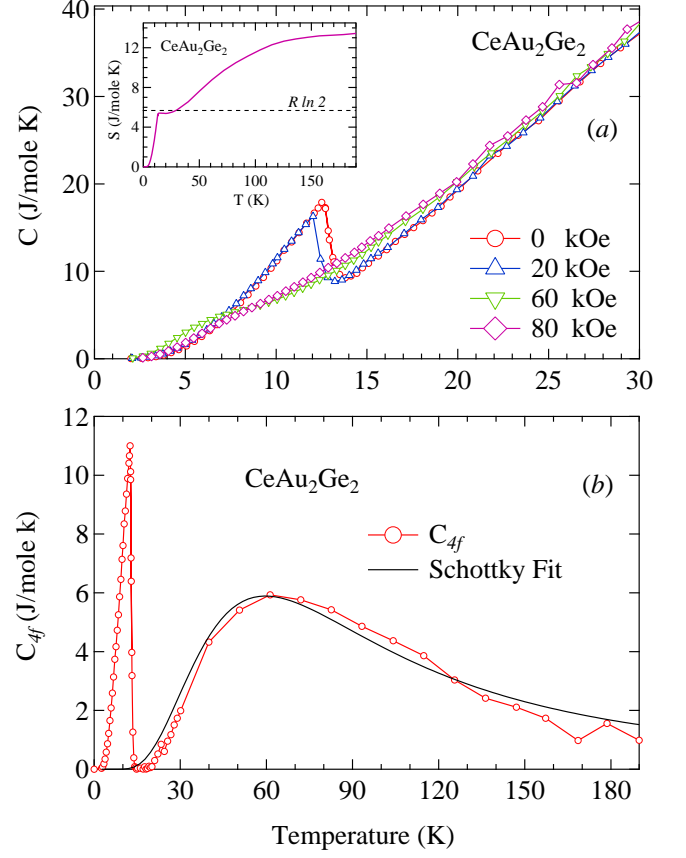


Figure 6: (Color online) a) Heat capacity of  $\text{CeAu}_2\text{Ge}_2$  in presence and absence of magnetic fields. The inset shows the  $4f$  entropy against temperature for the same. b) Magnetic contribution ( $C_{4f}$ ) to the heat capacity of  $\text{CeAu}_2\text{Ge}_2$  with a Schottky fit.

is 5.5 J/mol K at  $T_N$ , close to the value for a well isolated doublet ground state and attains a value of 13.4 J/mol K at 190 K, comparable to the theoretically expected value of  $R \ln 6$  (14.9 J/mol K).

In order to understand the magnetocrystalline anisotropy and to know about the crystal field energy level splittings of the  $\text{R}^{3+}$  ion in  $\text{RAu}_2\text{Ge}_2$ , we have performed the CEF calculations using the point charge model. The rare-earth atom in this series of compounds occupy the 2a Wyckoff position which has the tetragonal point symmetry. The CEF Hamiltonian for a tetragonal symmetry is given by,

$$H_{\text{CEF}} = B_2^0 O_2^0 + B_4^0 O_4^0 + B_4^4 O_4^4 + B_6^0 O_6^0 + B_6^4 O_6^4; \quad (6)$$

where  $B_m^n$  and  $O_m^n$  are the CEF parameters and the Stevens operators, respectively [22, 23]. The CEF susceptibility is defined as

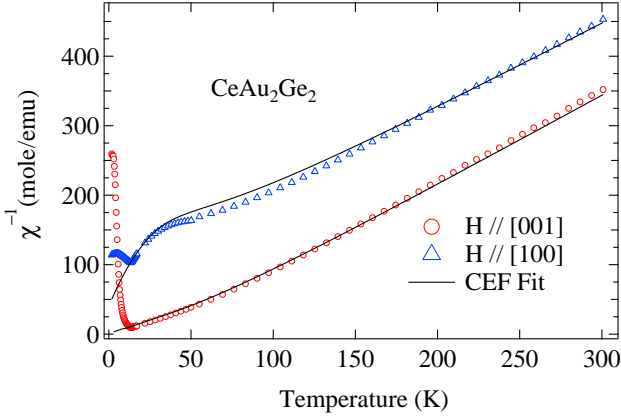


Figure 7: (Color online) Inverse susceptibility of  $\text{CeAu}_2\text{Ge}_2$  for  $H // [100]$  and  $[001]$  directions. The solid line through the data points represent the crystal electric field fit.

$$\chi_{\text{CEF}}^{-1} = N (g_J B)^2 \frac{1}{Z} \sum_{m,n} \frac{e^{-E_n}}{e^{-E_m}} \frac{\langle J_m | J_z | J_n \rangle^2}{\langle J_m | J_z | J_m \rangle \langle J_n | J_z | J_n \rangle} e^{-E_n} + \sum_n \frac{e^{-E_n}}{Z} \langle J_n | J_z | J_n \rangle^2 e^{-E_n} A; \quad (7)$$

where  $g_J$  is the Landé  $g$ -factor,  $E_n$  and  $J_n$  are the  $n$ th eigenvalue and eigenfunction, respectively.  $J_i$  ( $i=x, y$  and  $z$ ) is the component of the angular momentum, and  $\langle J_m | J_z | J_n \rangle = \langle J_m | J_z | J_n \rangle$ ,  $Z = \sum_n e^{-E_n}$  and  $A = 1/k_B T$ . The magnetic susceptibility including the molecular field contribution  $\chi_i$  is given by

$$\chi_i^{-1} = \chi_{\text{CEF}}^{-1} - \chi_i; \quad (8)$$

For  $\text{Ce}^{3+}$  ions the  $O_6$  terms in the above Hamiltonian vanishes resulting in only three crystal field parameters. The inverse susceptibility of  $\text{CeAu}_2\text{Ge}_2$  with field along both the crystallographic directions was fitted to the mentioned CEF model as shown in Fig. 7. The CEF parameters obtained for the best fit are  $B_2^0 = -6.4$  K,  $B_4^0 = -0.27$  K and  $B_4^4 = 2.6$  K with a molecular field contribution of  $\chi(100) = -41$  K and  $\chi(001) = -8$  K respectively for field along  $[100]$  and  $[001]$  directions. The negative value of  $\chi$  supports the antiferromagnetic exchange interaction among the moments. The susceptibility could be fitted using a set of values of CEF parameters but only those values were considered which could also fit the experimentally obtained Schottky anomaly. The CEF split energy levels obtained from the above CEF parameters are three doublets  $\epsilon_0 = 0$  K,  $\epsilon_1 = 128$  K and  $\epsilon_2 = 199$  K which are in excellent agreement with the values derived from neutron scattering results on polycrystalline sample. These energy levels were used to calculate the Schottky

contribution using the equation

$$C_{\text{Sch}}(T) = R \frac{\sum_i g_i e^{-E_i/T} \sum_i g_i E_i^2 e^{-E_i/T} \sum_i g_i E_i e^{-E_i/T}}{T^2 \sum_i g_i e^{-E_i/T}} \quad (9)$$

where  $R$  is a gas constant,  $E_i$  is the energy in units of temperature and  $g_i$  is the degeneracy of the energy level. The calculated Schottky heat capacity is in good agreement with the observed one as seen in Fig. 6b. According to the mean field theory, the CEF parameter  $B_2^0$  is related to the exchange constant and paramagnetic Curie temperature by the relation [24]

$$\chi_{\text{P}}^{[001]} = \frac{J(J+1)}{3k_B} J_{\text{ex}}^{[001]} - \frac{(2J-1)(2J+3)}{5k_B} B_2^0; \quad (10)$$

$$\chi_{\text{P}}^{[100]} = \frac{J(J+1)}{3k_B} J_{\text{ex}}^{[100]} + \frac{(2J-1)(2J+3)}{10k_B} B_2^0; \quad (11)$$

Substituting the values of the parameters we obtain  $J_{\text{ex}}^{[001]} = -14.5$  K and  $J_{\text{ex}}^{[001]} = -4.7$  K. The negative value of the exchange constant along both the principal directions imply an overall antiferromagnetic interaction among the moments.

Fig. 8a shows the temperature dependence of resistivity for  $\text{CeAu}_2\text{Ge}_2$  with current parallel to  $[100]$  and  $[001]$  directions. The resistivity shows a metallic behavior down to  $\sim 130$  K followed by a broad hump and then drops faster at the ordering temperature ( $T_N = 13.5$  K)

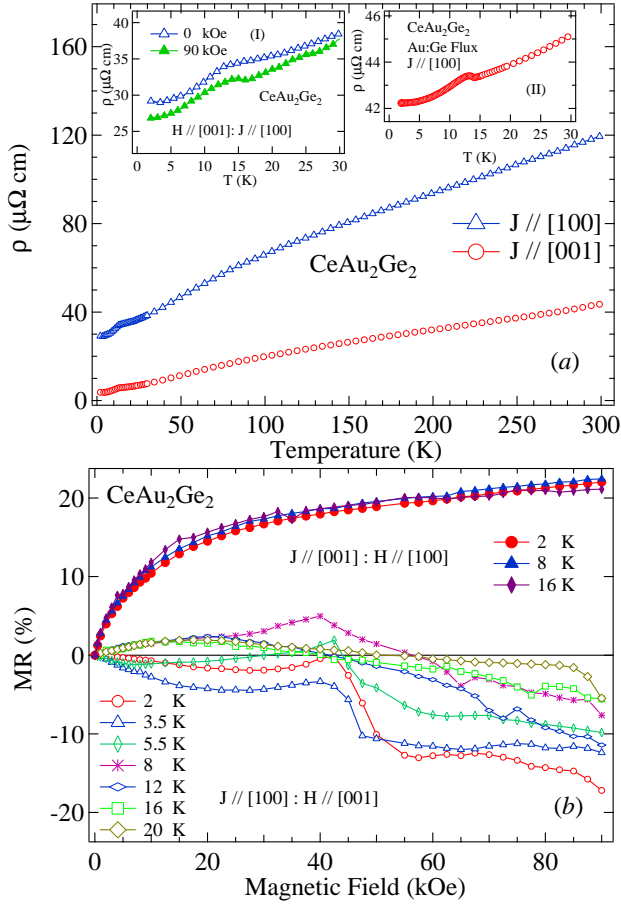


Figure 8: (Color online) a) Resistivity of  $\text{CeAu}_2\text{Ge}_2$  with  $J // [100]$  and  $[001]$  direction. The inset (I) shows the low temperature portion with  $J // [100]$  and  $H // [001]$  direction. The inset (II) shows the resistivity of  $\text{CeAu}_2\text{Ge}_2$  single crystal grown with Au:Ge flux ( $J // [100]$ ) for comparison with the presently studied Bi flux grown single crystal. b) The transverse magnetoresistance of the same with  $J // [100]$ ,  $H // [001]$  and  $J // [001]$ ,  $H // [100]$  at various temperatures are shown.

due to the gradual freezing of the spin disorder resistivity. The broad hump below 130 K is due to the CEF effects. The thermally induced variation of the fractional Boltzmann occupation of the CEF levels changes the otherwise constant spin disorder resistivity and is qualitatively in agreement with the calculated CEF split energy levels with second excited state lying at 199 K. Similar to  $\text{LaAu}_2\text{Ge}_2$  the resistivity with current along  $[100]$  direction is higher than along  $[001]$  indicating the structural anisotropy in this compound. The inset (I) of Fig. 8a shows the low temperature resistivity in zero and applied field of 90 KOe for  $J // [100]$  and  $H // [001]$ . The resistivity curve drops at the ordering temperature of the compound as usual. Application of magnetic field (90 KOe) reduces the resistivity with appearance of a hump just above the ordering temperature. The negative magne-

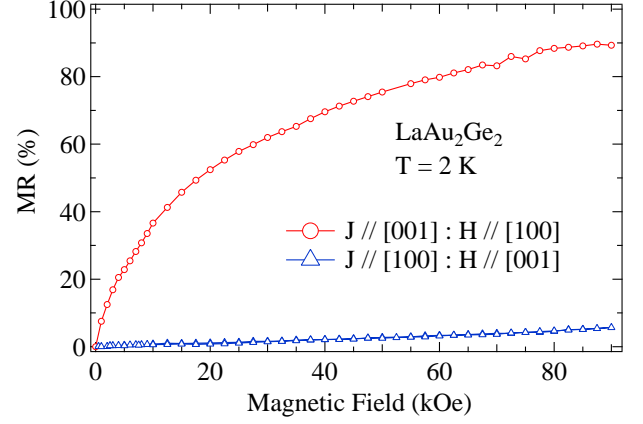


Figure 9: (Color online) Transverse Magnetoresistance of  $\text{LaAu}_2\text{Ge}_2$  at 2 K.

toresistance is in agreement with the (field induced) ferromagnetic behavior of the compound at 90 KOe. The negative magnetoresistance above the ordering temperature is due to the reduction in the spin disorder scattering in presence of field (90 KOe) compared to the zero field one. The appearance of hump just above the ordering temperature with application of field is an anomalous behavior. The exact reason for the observed behavior is not known but one of the possibilities is discussed below. At 90 KOe and low temperatures the compound is in the field induced ferromagnetic state, increase in temperature may result in the formation of short range spin fluctuations as a consequence of competition between the thermal energy and the external field causing the scattering of the conduction electrons.

The inset (II) of Fig. 8a shows the low temperature part of the resistivity ( $J // [100]$ ) of  $\text{CeAu}_2\text{Ge}_2$  single crystal grown using Au:Ge flux. Unlike the resistivity of Bi flux grown single crystal, the resistivity of Au:Ge flux grown crystal shows a peak at the ordering temperature  $T_N = 13.5$  K. This type of peak at the ordering temperature is generally attributed to the superzone gap effect. But considering the previous neutron diffraction studies which shows that  $\text{CeAu}_2\text{Ge}_2$  is a simple collinear antiferromagnet [15] with a propagation vector  $(0, 0, 1)$ , where such type of superzone gap effect are not usually observed, we claim that the single crystal grown using Bi-flux is good compared to the Au:Ge flux grown single crystals. Although, the other preliminary magnetic property of Au:Ge flux grown single crystal shows similar behavior (not shown here for brevity) to that of Bi flux grown single crystals.

The transverse MR resistance of  $\text{CeAu}_2\text{Ge}_2$  as a function of field and temperatures is shown in (Fig. 8b). The magnetoresistance of the compound was calculated using the relation  $\text{MR} = [\text{R}(H) - \text{R}(0)] / \text{R}(0)$  ( $\text{MR} \% = \text{MR} * 100$ ). Before discussing the MR behavior of  $\text{CeAu}_2\text{Ge}_2$  we first discuss the MR behavior of  $\text{LaAu}_2\text{Ge}_2$  (Fig. 9) which would be helpful in under-



standing the MR behavior of  $\text{CeAu}_2\text{Ge}_2$ . The MR of  $\text{LaAu}_2\text{Ge}_2$  with  $J \parallel [100]$  and  $H \parallel [001]$  (Fig. 9) increases with field up to 5 % at 90 KOe. Whereas with  $J \parallel [001]$  and  $H \parallel [100]$  the MR increases anomalously to 90 % at 90 KOe. The large anisotropic behavior in the MR of the nonmagnetic compound indicates the presence of significant anisotropy in the Fermi surface of the compound. Referring to the MR of  $\text{CeAu}_2\text{Ge}_2$  at 2 K and with  $J \parallel [100]$  and  $H \parallel [001]$ , the curve initially decreases with field followed by an upward turn above 30 KOe and then decreases sharply above 42 KOe. The initial decrease in MR at low fields (below 30 KOe) is surprising since the compound is in the antiferromagnetically ordered state and a positive magnetoresistance is generally expected. The negative magnetoresistance appears in the compounds having ferromagnetic ordering or Kondo behavior. The initial negative increase of MR at low fields indicates the weak Kondo interaction in the compound, but sufficient enough to overcome the small positive contribution arising from Lorentz effect and antiferromagnetic ordering. The presence of weak Kondo interaction is supported by the large negative value of  $\chi_p$ , low saturation moment of  $1.86 \mu_B/\text{Ce}$  in the magnetic isotherm at 2 K and a heat capacity jump of  $11 \text{ J/mol K}$  compared to  $12.5 \text{ J/mol K}$ . The upward turn in the MR between 30 and 42 KOe is due to the positive contribution arising from antiferromagnetic ordering. The sharp drop in the magnetoresistance above 42 KOe corresponds to the field induced ferromagnetic behavior of the compound, consistent with the metamagnetic transition in the magnetic isotherm. With increase in temperature to 3.3 K the MR at low fields become more negative compared to that at 2 K. The behavior is also in agreement with the Kondo behavior which exhibit a minimum in temperature variation of MR [25]. At high temperature (above 5.5 K) the MR increases with field due to the increasing positive contribution from antiferromagnetic coupling and decreasing contribution from Kondo effect. The maximum occurs at 8 K and then decreases with temperature as expected. The negative contribution in the paramagnetic state at high fields is due to the decrease in the spin disorder scattering. The MR with  $J \parallel [001]$  and  $H \parallel [100]$  is in sharp contrast to the former one showing a positive contribution at all fields and nearly temperature independent behavior. The temperature independent behavior of the MR indicates the absence of magnetic contribution. Comparing the MR behavior with that of the La counterpart and assuming that a similar applies here, it is possible that an anisotropy in the Fermi surface cause a comparatively large MR with  $J \parallel [001]$  suppressing the other smaller contribution. With  $J \parallel [100]$ , because of the smaller contribution from the Fermi surface, the other magnetic contributions are dominant.

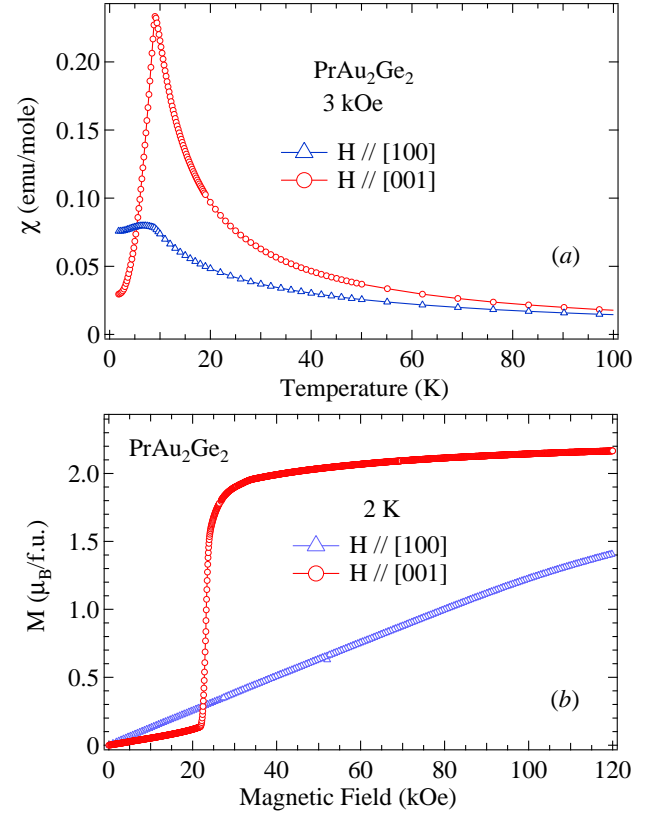


Figure 10: (Color online) a) Magnetic susceptibility of  $\text{PrAu}_2\text{Ge}_2$  with magnetic field (3kOe) applied along the two crystallographic directions. b) Magnetic isotherm at 2 K for the same with field along both the crystallographic directions.

### C. $\text{PrAu}_2\text{Ge}_2$

$\text{PrAu}_2\text{Ge}_2$  orders antiferromagnetically at 9 K with  $[001]$  as the easy axis of magnetization (Fig. 10a) similar to  $\text{CeAu}_2\text{Ge}_2$ . In the paramagnetic state, the magnetic susceptibility was fitted to the Curie-Weiss law. The fit gives  $\chi_p$  and  $\theta_p$  as  $3.57 \mu_B/\text{Pr}$  and  $-10 \text{ K}$  and  $10 \text{ K}$  for field parallel to  $[100]$  and  $[001]$  directions, respectively. The value of  $\chi_p$  is equal to the theoretically expected value of  $\text{Pr}^{3+}$  ion. The magnetic isotherm at 2 K (Fig. 10b) with  $H \parallel [001]$  shows a linear behavior up to 20 KOe in confirmation with the antiferromagnetic nature of the compound. At 22 KOe ( $H \parallel [001]$ ) the compound undergoes a spin flip type metamagnetic transition followed by slow increase with field attaining a magnetic moment of  $2.2 \mu_B/\text{f.u.}$  at 120 KOe. The moment is less than the saturation moment of  $\text{Pr}^{3+}$  ion. The less moment may be due to the crystal field effect. The magnetic isotherm with field along  $[100]$  direction increases linearly with a magnetization of  $1.4 \mu_B/\text{f.u.}$  at 120 KOe, indicating the hard axis of magnetization. The magnetic phase diagram constructed as discussed before (Fig. 11a) shows the antiferromagnetic and the



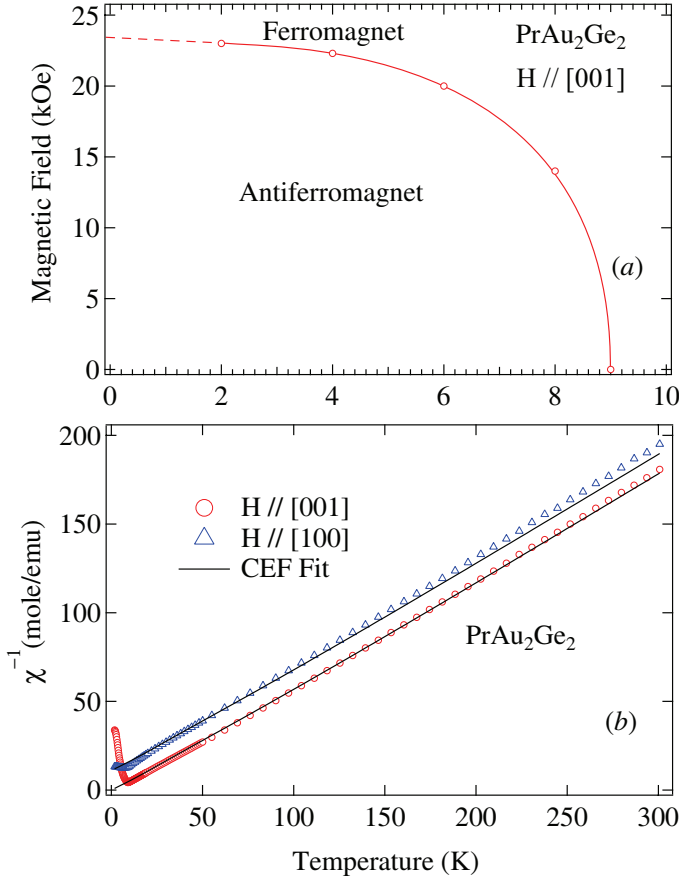


Figure 11: (Color online) a) Magnetic Phase Diagram of  $\text{PrAu}_2\text{Ge}_2$  constructed from the magnetic isotherms at various temperatures. b) Inverse susceptibility of  $\text{PrAu}_2\text{Ge}_2$  with crystal electric field fit.

field induced ferromagnetic behavior of the compound. For detailed investigation a crystal field analysis of the compound was done by fitting the inverse susceptibility as shown in Fig. 11b. The Obtained value of the crystal field parameters are  $B_2^0 = -1.2$  K,  $B_4^0 = 0.08$  K,  $B_4^4 = 0.25$  K,  $B_6^0 = -0.0001$  K and  $B_6^4 = 0.006$  K with a molecular field contribution of  $(100) = -10$  K and  $(001) = 0$  K respectively for field along  $[100]$  and  $[001]$  directions. Only those value of crystal field parameters are considered which fits the susceptibility as well as provide a satisfactory representation of the Schottky anomaly inferred from the heat capacity measurements (described below). The crystal field split energy levels calculated using the above crystal field parameters are  $4_0 = 0$  K (doublet),  $4_1 = 39$  K,  $4_2 = 98$  K,  $4_3 = 115$  K,  $4_4 = 148$  K,  $4_5 = 186$  K (doublet) and  $4_6 = 261$  K. The energy level scheme shows a doublet ground state for the  $\text{Pr}^{3+}$  ion. The exchange interaction constant obtained using Eq. 11 and 10 are  $J_{\text{ex}}^{[100]} = -0.114$  K and  $J_{\text{ex}}^{[001]} = -1.27$  K. The negative value of the exchange interaction constant along both the direction indicates an overall antiferromagnetic interaction among the moments

The heat capacity behavior of  $\text{PrAu}_2\text{Ge}_2$  in 0, 20 and

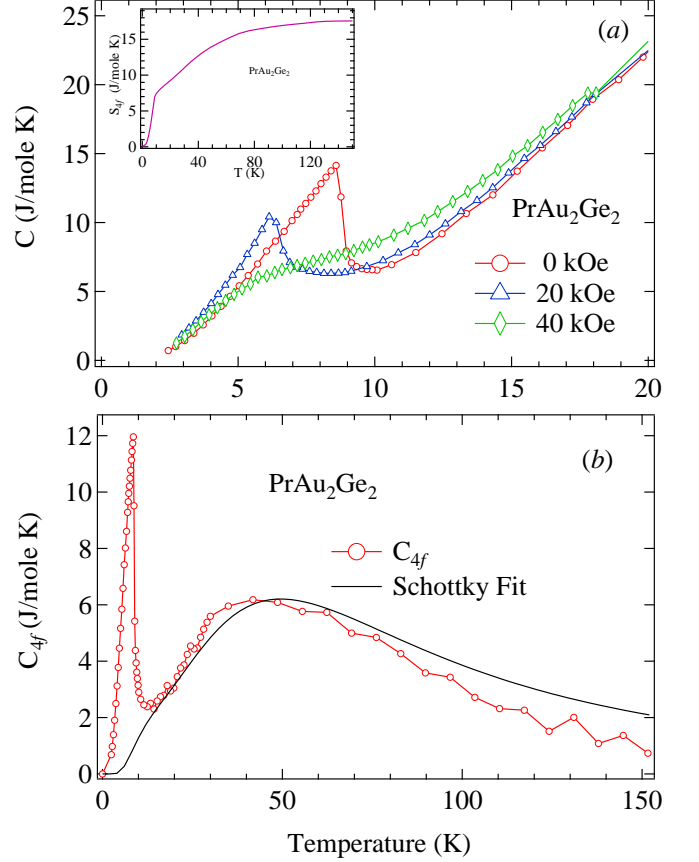


Figure 12: (Color online) a) Heat capacity of  $\text{PrAu}_2\text{Ge}_2$  in 0, 20 and 40 KOe. The inset shows the  $4f$  entropy against temperature. b) Magnetic contribution ( $C_{4f}$ ) to the heat capacity of  $\text{PrAu}_2\text{Ge}_2$ ; the solid line shows the Schottky heat capacity calculated from the CEF levels.

40 KOe is shown in Fig. 12a. The heat capacity shows an anomaly at the antiferromagnetic ordering temperature of the compound. An external field of 20 KOe shifts the peak towards low temperature as expected for an antiferromagnetically ordered compound. At a higher field of 40 KOe, above the metamagnetic transition field, the peak vanishes and there is a broad hump. The magnetic contribution to the heat capacity (Fig. 12b) was isolated by subtracting the heat capacity of  $\text{LaAu}_2\text{Ge}_2$ . It shows a sharp peak at the ordering temperature followed by a Schottky anomaly at high temperature. The entropy calculated using the equation as mentioned before is plotted as a function of temperature in the inset of Fig. 12a. It attains a value of  $7$  J/mol K at the ordering temperature, which exceeds substantially the entropy for a doublet ground state with effective  $J = 1/2$  ( $5.76$  J/mol K). The excess entropy appears because of a substantial contribution to  $C_{4f}$  due to the Schottky heat capacity at low temperatures arising from the first excited CEF level lying at  $39$  K. The total entropy obtained at  $150$  K is  $17.6$  J/mol K, close to the expected

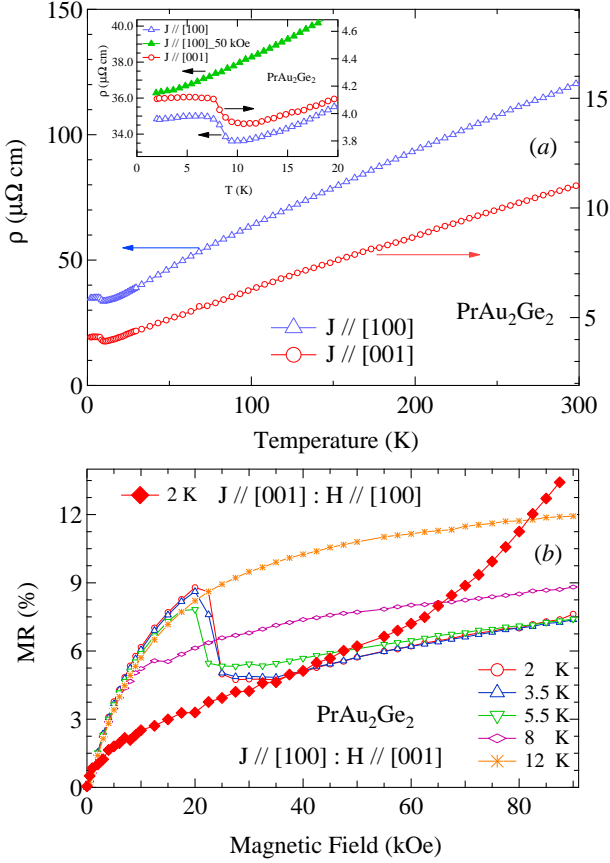


Figure 13: (Color online) a) Resistivity of  $\text{PrAu}_2\text{Ge}_2$  with  $J // [100]$  and  $[001]$  direction. The inset shows the expanded low temperature portion with arrows indicating the respective axis. b) The transverse magnetoresistance of the same with  $J // [100]$ ;  $H // [001]$  at various temperatures and  $J // [001]$ ;  $H // [100]$  are shown.

value of  $18.2 \text{ J/mol K}$ . The solid line in Fig. 12b shows the Schottky heat capacity calculated from the CEF split energy levels using expression 9. An overall good agreement with the experimental  $C_{4f}$  increases the confidence in the proposed CEF level scheme.

The resistivity of  $\text{PrAu}_2\text{Ge}_2$  with current along the two principle crystallographic directions is shown in Fig. 13a. The resistivity with  $J // [100]$  is higher than that with  $J // [001]$  as seen for both La and Ce compounds. The resistivity with current along both the directions show a metallic behavior down to the ordering temperature (inset of Fig. 13a.) and then falls down marginally at low temperatures. The behavior is anomalous to the one expected below the ordering temperature. The rise of the resistivity at the ordering temperature is attributed to the formation of energy gap in conduction band due to the difference in the periodicity of the antiferromagnetic configuration and lattice, also Known as superzone gap effect [26]. The behavior indicates that moments have

antiferromagnetic interaction along both the directions with different periodicity. Since the resistivity with  $J // [100]$  is higher than that with  $J // [001]$  and also the rise in the resistivity at  $T_N$  is  $1.5 \text{ m}\Omega \text{ cm}$  for the former case and  $0.3 \text{ m}\Omega \text{ cm}$  for the later, we infer a higher energy gap along the  $[100]$  direction compared to that along  $[001]$  direction. The superzone gap effect in few cases affects the Fermi surface and reduces the density of states at the Fermi level resulting in the marginal decrease of the resistivity below  $T_N$ . In an applied field of 50 KOe (field well above the metamagnetic transition) the upturn in the resistivity at  $T_N$  vanishes due to the disappearance of superzone gap effect and the resistivity decreases linearly for both the direction (shown only for  $J // [100]$ ;  $H // [001]$ ) of current.

The transverse MR of the compound at various temperatures is shown in Fig. 13b. The magnetoresistance at 2 K and with  $J // [100]$  and  $H // [001]$  initially increases with field up to  $20 \text{ KOe}$  followed by a sharp drop and then increases at higher field. The sharp drop in MR is due to the field induced ferromagnetic behavior of the compound. The sharp drop moves towards lower field with increase in temperature as expected and vanishes in the paramagnetic state (12 K). The initial increase of the positive MR with field (below  $20 \text{ KOe}$ ) reflects contributions from both the fluctuations induced in the antiferromagnetic state by the applied field and positive Lorentz contribution from the conduction electrons. The latter is also likely responsible for the increase of MR at higher fields and low temperatures. Its presence is also evident from the MR at 12 K (paramagnetic state) which increases and saturates at high fields. With  $J // [001]$  and  $H // [100]$  the MR increases with field followed by an increase in the slope at higher fields (above  $60 \text{ KOe}$ ). The increase in the slope at high fields may be due to the gradual orientation of the ordered moments towards  $[100]$  direction.

#### IV. CONCLUSION

In conclusion, we have studied the magnetic behavior of the single crystalline  $\text{RAu}_2\text{Ge}_2$  (R La, Ce and Pr) compounds.  $\text{LaAu}_2\text{Ge}_2$  shows a Pauli-paramagnetic behavior with both resistivity and heat capacity measurements reflecting its nonmagnetic behavior. The heat capacity shows a presence of both optical and acoustic modes of vibration of its atoms. The magnetoresistance behavior indicates a large anisotropy in the geometry of its Fermi surface.  $\text{CeAu}_2\text{Ge}_2$  shows a simple antiferromagnetic behavior with  $T_N = 13.5 \text{ K}$  and  $[001]$  as the easy axis of magnetization. The compound undergoes a spin flip like metamagnetic transition at  $2 \text{ K}$  and at a critical field  $H_C = 43 \text{ KOe}$  driving the compound to a field induced ferromagnetic state. The low temperature behavior of the compound indicates a presence of weak Kondo interaction.  $\text{PrAu}_2\text{Ge}_2$  orders antiferromagnetically at  $T_N = 9 \text{ K}$  with  $[001]$  as the easy axis of magnetization.

This compound also undergoes a spin flip type metamagnetic transition at 2 K and at a critical field  $H_C$  22 KOe. Crystal electric field analysis for  $CeAu_2Ge_2$

and  $PrAu_2Ge_2$  shows a doublet ground state for both the compounds.

- 
- [1] W. Franz, A. Griebel, F. Steglich, and D. Wohlleben, Z. Physik B **31**, 7 (1978).
  - [2] G. Knopp, A. Loidl, K. Knorr, L. Pawlak, M. Duczmal, R. Caspary, U. Gottwick, H. Spille, F. Steglich, and A.P. Murani, Z. Phys. B - Condensed Matter **77**, 95 (1989).
  - [3] J. Yoshida, S. Abe, D. Takahashi, Y. Segawa, Y. Komai, H. Tsujii, K. Matsumoto, H. Suzuki and Y. Onuki, Phys. Rev. Lett. **101**, 256402 (2008).
  - [4] N. D. Mathur, F. M. Grosche, S. R. Julian, I. R. Walker, D. M. Freye, R. K. W. Haseiwimmer and G. G. Lomzarich, Nature (London), **394**, 39 (1998).
  - [5] E. Vargoz and D. Jaccard, J. Magn. Magn. Mater., **177**, 294 (1998).
  - [6] R. Movshovich, T. Graf, D. Mandrus, J. D. Thompson, J. L. Smith, and Z. Fisk, Phys. Rev. B **53**, 8241 (1996).
  - [7] A. Thamizhavel, R. Kulkarni, and S. K. Dhar, Phys. Rev. B **75**, 144426 (2007).
  - [8] A. M. Mulders, A. Yaouanc, P. Dalmas de Reotier, P. C. M. Gubbens, A. A. Moolenaar, B. Fak, E. Ressouche, K. Prokes, A. A. Menovsky, and K. H. J. Buschow, Phys. Rev. B **56**, 8752 (1997).
  - [9] J. Vejpravova, J. Prokleska, V. Sechovsky, J. Magn. Magn. Mater., **316**, e374 (2007).
  - [10] A. Szytula, J. Leciejewich, H. Binzycka, Phys. Stat. Sol. A **58**, 67 (1980).
  - [11] T. Kawae, M. Mito, M. Hitaka, F. Ichikawa, T. Shigeoka, N. Iwata and K. Takeda, J. Phys. Soc. Jpn. **69**, 586 (2000).
  - [12] J. A. Blanco, R. M. Nicklow and D. Schmitt. Physica B **213**, 327 (1995).
  - [13] E. Wawrzynska, M. Bałanda, S. Baran, J. Leciejewicz, B. Penc, N. Stüfer and A. Szytula, J. Phys.:Condens. Matter **17** 1037 (2005).
  - [14] K. Hiebl, C. Horvath, P. Rogl, M. J. Sienko, Solid State Comm. **48**, 211 (1983).
  - [15] A. Loidl, K. Knorr, G. Knopp, A. Krimmel, R. Caspary, A. Bohm, G. Sparn, C. Geibel, F. Steglich, A. P. Murani, Phys. Rev. B **46**, 9341 (1992).
  - [16] K. Nishimura, M. Yamamoto, K. Mori, J. Magn. Magn. Mater., **177-181**, 1087-1088 (1998).
  - [17] J. Rodrigues-Carvajal, Physica B (Amsterdam) **192**, 55 (1992).
  - [18] FR de Boer, J. C. P. Klaasse, P. A. Veenhuizen, A. Bohm, C. D. Bredl, U. Gottwick, H. M. Mayer, L. Pawlak, U. Rauchschwalbe, H. Spille and F. Steglich, J. Magn. Magn. Mater., **63-64**, 91-94 (1987).
  - [19] W. N. Lawless, Phys. Rev. B **14**, 134 (1976).
  - [20] R. G. Chambers, Proc. Phys. Soc. London **78**, 941 (1961).
  - [21] E. S. R. Gopal, Specific Heat at Low Temperatures, (Plenum Press), **Chap. 2** (1966) and references therein.
  - [22] K. W. H. Stevens, Proc. Phys. Soc., London, Sect. A **65**, 209 (1952).
  - [23] M. T. Hutchings, in *Solid State Physics: Advances in Research and Applications*, edited by F. Seitz and B. Turnbull (Academic, New York, 1965), Vol.16, p.227.
  - [24] J. Jensen and A. R. Mackintosh, Rare earth magnetism structures and excitations, Calrendon press, Oxford **Chap 2**, p. 73 (1991).
  - [25] V Zlatic, J. Phys. F: Met. Phys. **11**, 2147 (1981)
  - [26] R. J. Elliot and F. A. Wedgwood: Proc. Phys. Soc. **81**, 846 (1963).